Application Note AN2047

Ultrasound Motion Sensor

By: Victor Kremin
Associated Project: Yes
Associated Part Family: CY8C26443

Summary
The Doppler-Effect-based ultrasound motion detection sensor is proposed. The sensor is primarily intended to be used in security systems for detection of moving objects, but can be effectively involved in intelligent children's toys, automatic door opening devices, and sports training and contact-less-speed measurement equipment.

Introduction
Modern security systems utilize various types of sensors to detect unauthorized object access attempts. The sensor collection includes infrared, microwave and ultrasound devices, which are intended to detect moving objects. Each type of sensor is characterized by its own advantages and drawbacks. Microwave sensors are effective in large apartments because microwaves pass through dielectric materials. But these sensors consist of expensive super-high frequency components and their radiation is unhealthy for living organisms.

Infrared sensors are characterized by high sensitivity, low cost and are widely used. But, these sensors can generate false alarm signals if heating systems are active or temperature-change speed exceeds some threshold level. Moreover, infrared sensors appreciably lose sensitivity if small insects penetrate the sensor lens.

Ultrasound motion detection sensors are characterized by small power consumption, suitable cost and high sensitivity. That it why this kind of sensor is commonly used in home, office and car security systems. Existing ultrasound sensors consist of multiple passive and active components and are relatively complicated for production and testing. Sensors often times require a laborious tuning process. The proposed sensor uses a single PSoC MCU together with few passive components. It is characterized by high sensitivity and resistance to various noise signals.

First of all, let us describe the basic principles of ultrasound motion detection sensor operation. Figure 1: Basic Sensor Operation Principle depicts the typical sensor installation:

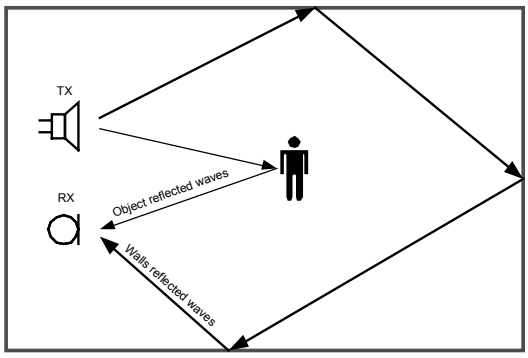

Figure 1: Basic Sensor Operation Principle

The ultrasound transmitter **TX** is emitting ultrasound waves into sensor ambient space continuously. These waves are reflecting from various objects and are reaching ultrasound receiver **RX**. There is a constant interference figure if no moving objects are in the placement.

Any moving object changes the level and phase of the reflected signal, which modifies the summed received signal level. Most low-cost sensors (car security systems, for instance) perform reflected signal amplitude analysis to detect moving objects. In spite of implementation simplicity, this detection method is characterized by a high sensitivity to noise signals. For example, heterogeneous airflows, sensor vibrations, room window and door deformations, and gusts can change the interference figure and generate false alarm signals.

Better noise resistance may be obtained if the receive sensor is performing reflected signal frequency analysis instead of amplitude examination. The reflected signal spectrum emulates a Doppler Effect. Frequency components of the moving object speed vector have a component in the direction of ultrasound radiation propagation. Because ultrasound waves reflect from the windows, walls, furniture etc., the sensor can detect object movements in any direction. To implement this principle, the sensor must perform selection and processing of Doppler Effect frequency shift to detect moving objects.

The air condition systems, heat generators, and refrigerators typically include movable parts, which can cause device vibrations that generate high-frequency Doppler components in the reflected ultrasound signal. The heterogeneous variable temperature airflows are characterized by different ultrasound propagation speed that can raise low-frequency Doppler components in the reflected signal. That is why the noise-resistant motion detection sensor should limit the Doppler signals' frequency range from lower and upper bounds to satisfactory false-alarm free operation.

The ultrasound motion detection sensor has been developed in compliance with operation principles considered above. The table below summarizes the main sensor characteristics.

Table 1: Main Sensor Characteristics

Item	Item Value
Operation Range	5 cm – 4 m
Operation Frequency	30-50 kHz, determined by piezoelectric sensor resonant frequency
Power Consumption	27 mA (alarm off) 55 mA (alarm on)
Sensor Outputs	Alarm LED and relay with normal closed and normal open contact pairs
Sensor Response Time	0.25 s
The Range of Detected Object's Speed	10 cm/s – 1.5 m/s

The Sensor Flowchart

The sensor flowchart is illustrated in Figure 2: Sensor Block Diagram. Note that the gray blocks are used to mark the external units for the PSoC microcontroller. The sensor operates in the following way:

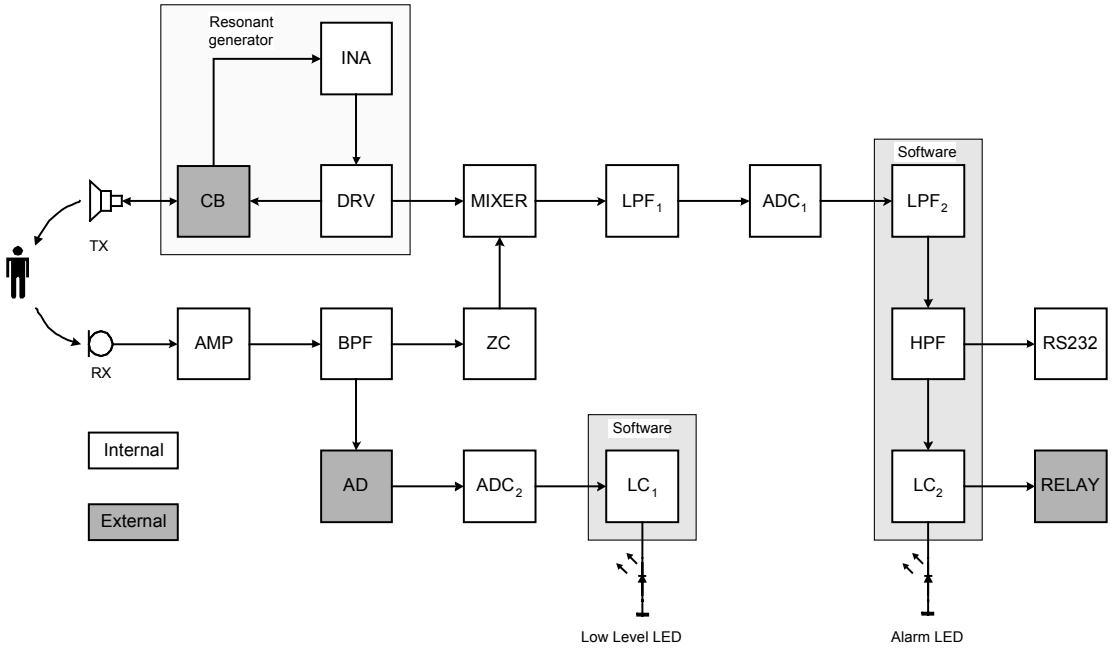

Figure 2: Sensor Block Diagram

The resonant generator drives the piezoelectric transmitter **TX**, which converts the electric signals into acoustic waves. The waves reflected from various objects reach the piezoelectric receiver **RX**, are converted into electric signals and amplified by input amplifier **AMP**. The resonant band-pass filter **BPF** suppresses the off-band noise signals and removes the DC component from the input amplifier output signal.[1] As we considered above, the reflected signal can be amplitude modulated. Zero-crossing detector **ZC** suppresses this unwanted amplitude modulation, and converts the filter output signal into phase modulated signal. Note that if the amplitude for the signal reflected from the moving objects is smaller than for the signal reflected from fixed items, the band-pass filter output signal will be phase modulated. It will be frequency modulated in the opposite case. In the security system, the signal reflected from moving objects can be 3 to 20 times weaker than the signal reflected from unmoved objects.

The output of zero-crossing detector **ZC** is routed to signal input of the **MIXER**. The ultrasound generator output signal serves as the **MIXER** reference signal. The low-pass filter **LPF_1** selects the Doppler signal from the mixer products. Filter output signal is then sampled by sigma-delta **ADC_1** for subsequent processing in the software. The software-implemented digital low-pass filter **LPF_2** additionally suppresses high-frequency components in Doppler signal frequency spectrum and removes the influence of zero-crossing detector phase noise.[2] Digital high-pass filter **HPF** limits the lower frequency in the Doppler spectrum. It effectively suppresses the influence of low-frequency noise signals on sensor operation. The high-pass, filter-output signal is analyzed by the level comparator **LC_2** for alarm signal generation. For alternative sensor applications or testing purposes, the filtered data stream can be transmitted via an RS232 compatible transmitter.

For reliable detection of movable objects, the reflected waves' signal level must be larger than some predefined value. If this condition is not satisfactory, the sensor must be placed in another location or transmitter output power must be increased. The input level controlling subsystem consists of amplitude detector **AD**, integrating analog-to-digital converter **ADC_2** and level comparator **LC_1**.

[1] The offset level of input amplifier can raise the DC component up to 0.75 V.

[2] In author's opinion, this noise is caused by **BPF** operational amplifier's noise and by PSoC digital part noise.

The piezoelectric sensors are characterized by a high Q factor and need precision tuning of operation frequency to achieve the maximum efficiency. Moreover, the sensor resonant frequency is temperature dependent and influenced by aging. As a result, expensive frequency and temperature compensation circuits are present in most ultrasound sensors today. Additionally, the piezoelectric sensors need relatively large input voltages for obtaining the demanded acoustic output power. These difficulties can be eliminated if a resonant generator is used in conjunction with a piezoelectric transmitter to stimulate bridge-load driver. If the same sensor is used for the receiver part, the temperature and aging effects on sensor performance is virtually eliminated.

The proposed sensor includes the resonant generator with a bridge transmitter for achieving maximum output power for given supply voltage. This generator consists of the piezoelectric driver **DRV**, a sensor current bridge **CB** for measuring crystal current, and instrumentation amplifier **INA**.

The Sensor Hardware

First, the detailed circuit diagram will be analyzed, then possible project improvements and design variations will be considered.

The Sensor Schematics

The complete sensor schematic is represented in Figure 3: Sensor Schematic; Analog Components and Figure 4: Sensor Schematic; CPU. Figure 3 depicts the analog components and Figure 4 represents the CPU.

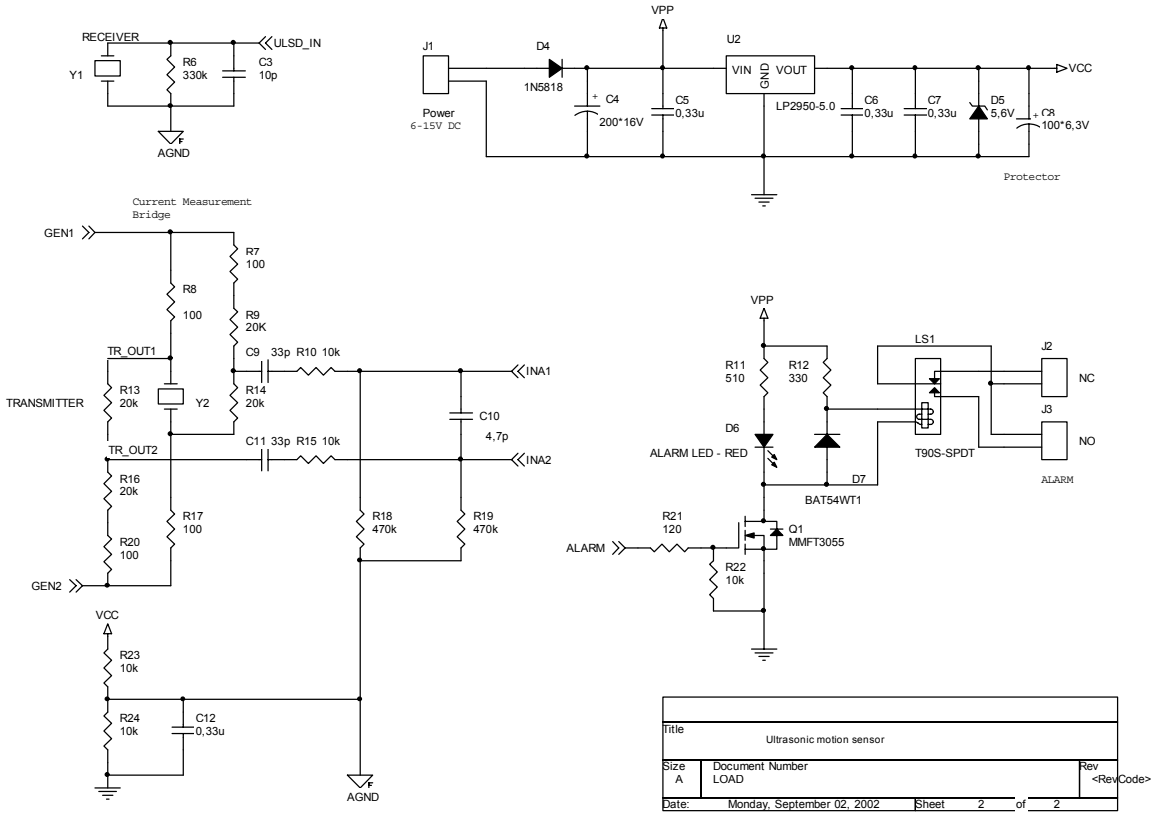

Figure 3: Sensor Schematic; Analog Components

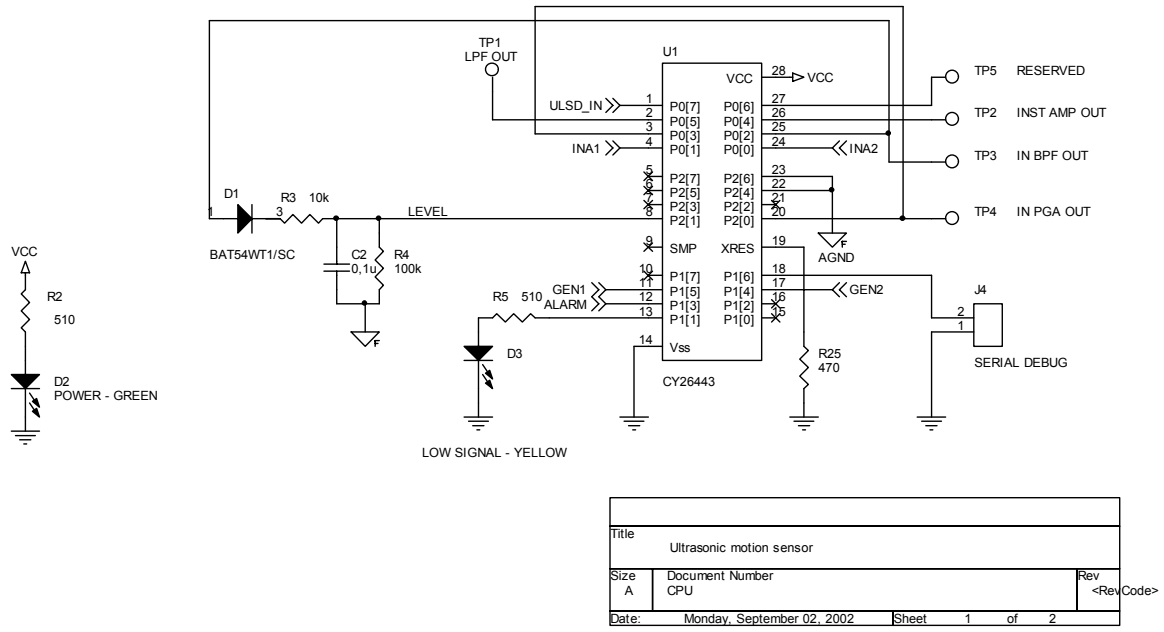

Figure 4: Sensor Schematic; CPU

The transmitter sensor current bridge has been formed by R_7-R_9, R_{13}-R_{14}, R_{16}-R_{17} and R_{20}. If $R_8 + R_{13} = R_{16} + R_{20}$ and $R_7 + R_9 = R_{14} + R_{17}$ then the voltage between the left pins of C_9 and C_{11} is directly proportional to the current in the piezoelectric transmitter Y_2. The differential networks, $C_9R_{10}R_{18}$ and $C_{11}R_{15}R_{19}$, compensate the phase shift in the internal PSoC MCU instrumentation amplifier and provide oscillation frequency very close to the main crystal resonance frequency. The network parameters are optimal for an oscillation frequency of 30-40 kHz and can be adjusted for other crystal's resonant frequencies. The sensor input stage has been formed by R_6C_3, so the $R_{23}R_{24}C_{12}$ determines the analog ground potential. The alarm relay is controlled by the Q_1 MOSFET. The other load types (such as open-drain output, solid state relay, buzzer, etc.) can be supported as well. The power supply consists of conventional linear regulator U_2. The diode D_4 protects the sensor electronics under reverse power conditions. The sensor can be powered from non-stabilized 6-12 V DC/AC supply with maximum current of 100 mA. Normal operation current is several times smaller.

The $D_1R_3C_2R_4$ form the amplitude detector for measuring the reflected signal level. LED D_3 indicates the low level of this signal. Connector J_4 brings the compatible CMOS serial transmitter output and can be used for sensor firmware debugging or alternative sensor applications.

To send this data stream to PC COM port for analysis, a standard level translator such as MAX3221 must be added externally.

The testpoints TP_1-TP_5 are intended for observing some PSoC MCU internal signals. The table below describes each testpoint function:

Table 2: Testpoint Descriptions

Testpoint Reference	Function
TP1	Output of switching capacitor low-pass filter, LPF_1 accordingly to Figure 2: Sensor Block Diagram
TP2	Output of generator instrumentation amplifier, INA
TP3	Output of band-pass filter, BPF
TP4	Output of receiver preamplifier, AMP; input of band-pass filter, BPF
TP5	Reserved for future extensions

The Chip Internals

The total chip interconnection is presented in Figure 5: PSoC MCU Internals. The port labels in brackets display the corresponding port numbers. The italic font depicts the matching net names and narrow lines have been used for presenting the clock lines. Gray color marks the unused blocks, which can be used to implement additional features.

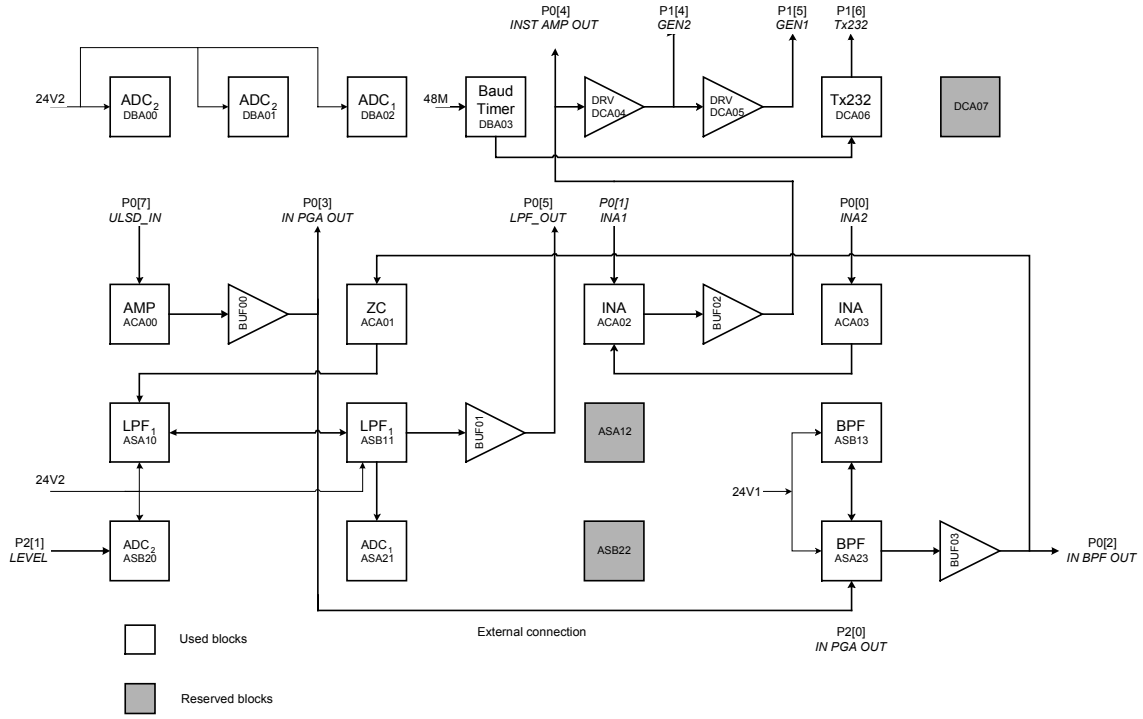

Figure 5: PSoC MCU Internals

The resonant generator consists of the instrumentation amplifier, which is placed into ACA02 and ACA03 analog continuous time blocks. The amplifier output is routed via internal PSoC Schmitt Trigger to input the first inverter, which has been placed into DCA04. The inverter output is connected to both piezoelectric crystal current bridge and the input of the second inverter, which has been placed in DCA05. The inverters form the bridge piezoelectric transmitter driver which allows for obtaining the maximum output power for the given supply voltage.

The sensor input signal is amplified by programmable gain amplifier (**PGA**) placed into ACA00 and is filtered by vertical band-pass filter placed into ASB13 and ASA23. The filter center frequency is selected to be at the piezoelectric transmitter resonant frequency. The maximum sample ratio is equal to 30, which is sufficient. The PGA output is connected externally with filter input; the PSoC routing and placement limitations prohibit making this connection internally. The programmable gain amplifier placed into ACA01 has been reconfigured as a zero-crossing detector by removing the operational amplifier feedback. For applications that demand an accurate spectrum analysis of Doppler-Effect signal, the **PGA** can be used directly by removing re-configuration code in software sources.

The mixer is combined with switched-capacitor low-pass filter **LPF_1**, which has been placed into ASA10 and ASB11 blocks. The amplitude modulation possibility of ASA10 block is used for the mixer operation. The mixer reference signal is brought in via *Global Output Bus 4* from the resonant generator. The filter output signal is routed via internal buffer to **P0[5]** port for debugging and testing purposes. Note that the LPF_1 filter cut-off frequency is selected to be 1200 Hz and the maximum sample ratio is near 140 for good suppression of ultrasound-carrier conversion high-frequency products.

The **LPF_1** filter output signal is sampled by the 8-bit sigma delta **ADC_1** and the subsequent processing is being done in software. The sigma-delta ADC selection is based on low CPU overheads and good AC characteristics. The **ADC_1** sample rate is 2.6 kHz. To measure the reflected signal level, the incremental 12-bit ADC is used. The ADC conversion time is the longest among other ADC types for given clock frequency, which allows effective suppressing of the unwanted reflected signal amplitude modulation. In our case, **ADC_2** sample rate is near 40 Hz.

The timer placed into DBA03 forms the baud rate signal serial transmitter that has been placed into DCA06. The **ADC_1** data stream can be passed via COM port to a PC for analysis or processing in sensor-alternative applications.

The Sensor Firmware

The sensor analyzes the Doppler-Effect signal continuously and turns on the alarm if the value of this signal within the inspected frequency range is bigger than some threshold value. The sensor software is implemented using the interrupt-main loop programming technique. The real-time data collection and processing algorithms are implemented in the **ADC_1** interrupt routine. Analysis of reflected signal level and sending the **ADC_1** data stream are implemented in the main software loop. The software sources allow building two software versions; debug and release dependent on the *DEBUG* variable definition. The debug software version sends the **ADC_1** filtered data stream via the serial transmitter together with other debug information. In the release version, these features are omitted which reduces power consumption and saves code space.

The main loop is quite simple. After reset, peripheral devices are initiated and data collection is started. Then, the level measuring **ADC_2** samples the sensors and updates the low-level LED status. Finally, the **ADC_1** sample status is checked and sent via serial port, if the debug software version has been built.

The data processing algorithms are implemented in the **ADC_1** interrupt routine. First, we perform the low-pass filtering for removing the high-frequency noise from Doppler-Effect signal. Next, we direct the low-pass filter output data stream to the high-pass filter to remove the lower frequency spectrum portion, which is done to improve the sensor noise resistance. Lastly, we perform the amplitude analysis of the high-pass filter output to detect the alarm signals. The alarm is turned on when the predefined number of interrupt cycles of the alarm condition has been detected.

The digital filters are implemented as finite impulse response (FIR) filters using the PSoC MCU multiple-accumulation unit (MAC). The low-pass filter operates at the **ADC_1** sample rate, and the filter cut-off frequency is set near 300 Hz. The filter length was selected to 11 taps. The high-pass filter operates at a quarter of the ADC sample rate with cut-off frequency of approximately 20 Hz. The filter length was chosen to 15 taps for reliable operation under indoor and outdoor conditions, but could be reduced to 7 in a less noisy environment.

The corresponding conditional compilation variable, **BPF_HIGH**, is present in the software source. Note that the lower sample rate of the FIR **HPF** was selected to provide the low cut-off frequency with smaller number of filter taps. Because the high-pass filter operates at a quarter sample rate, the Interrupt Service Routine (ISR) structure was optimized to provide balancing of CPU resources.

Because the high-pass filter operates with a lower sample rate, the **LPF_2** output does not require sampling on every interrupt. So, in the first interrupt time we calculate the **LPF_2** sample, next process this sample via digital **HPF** and perform the **HPF** output analysis in third interrupt routine call. Note that the **LPF_2** circular buffer must be updated each time. Figure 6: Data Processing Interrupt Routine Structure illustrates the proposed algorithm:

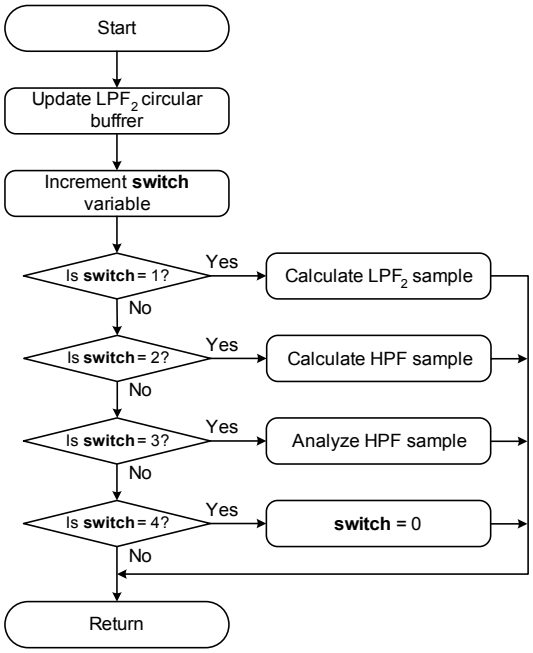

Figure 6: Data Processing Interrupt Routine Structure

To detect alarm events, a software peak detector has been implemented. Alternatively, a true RMS detector can be easily implemented using the PSoC MAC. No difference between these two approaches was observed.

The current version of the sensor firmware is relatively simple. It consumes only 3 Kbytes of code and 60 bytes of data RAM. The rest of the code and data memory is at user disposal and can be utilized for embedding the proposed sensor into various applications. For example, the author has combined this sensor with a doorbell for automatic sound level and melody changing when anyone comes close to the home entrance door. The PSoC MCU dynamic re-configuration possibility allows on-the-fly dynamic changing of PSoC functions and use of previously allocated hardware resources for alternative purposes.

The current software release was written in 'C' and runs at 12 MHz. We expect that assembly level optimization will allow the decrease of the CPU clock frequency two or more times for additional reduction in power consumption.

Design Variances and Sensor's Alternative Applications

The proposed sensor hardware and software were optimized for security system applications. For some types of these applications, the obtained operation range is unacceptable. For achieving larger operational distances, we recommend combining an external-power amplifier with a low-noise preamplifier. The standard MOSFET driver is ideally suitable for piezoelectric sensor driving because it is intended to drive large capacitance loads. The preamplifier will amplify the low-level signals. Figure 7: External Amplifiers for Longer Operational Range depicts the proposed schematic of this unit. The proposed amplifier is characterized by a maximum gain on the piezoelectric sensor resonant frequency, which allows suppression of the off-band noise signals.

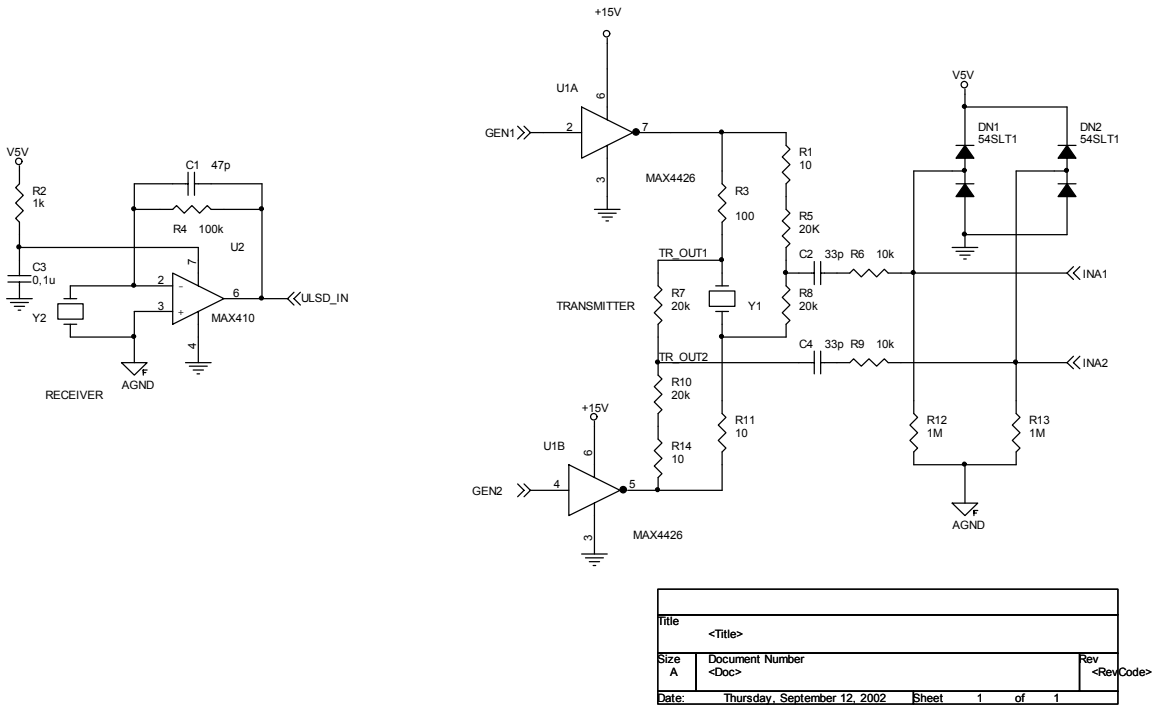

Figure 7: External Amplifiers for Longer Operational Range

Next, let us describe the resonant generator variants. We use the PSoC MCU internal Schmitt Trigger for converting the amplifier analog signal into digital. Alternatively, the signal from *Comparator Bus 2* can be routed to *Global Output Bus 5*[3] via the SPIS User Module.

This approach has been tested but we observed larger power consumption and jitter on generated waveform.

[3] SPIS is a non-inverting module, so we must first route the signal to *Global Output Bus 5* and later to *Global Output Bus 4* via digital inverter to preserve existing sensor schematic.

The scope of sensor applications is not limited to security systems. These applications can be used for movement activated intellectual children toys, automatic door opening systems, identification system, etc. Secondly, the sensor can be used for remote, contact-less speed measurement and machined parts-vibration analysis. For example, the sensor can be built into various sports training equipment for controlling the practice pace and optimizing the training load time distribution.

For speed measurement applications, the speed can be determined by measuring the frequency of the Doppler-Effect signal. The methods that can be used include the "classic" counter frequency/period measuring method, FFT or correlation technique, wavelet transformation-based analysis, etc. The wavelet transformation is optimal for analyzing non-stationary signals.

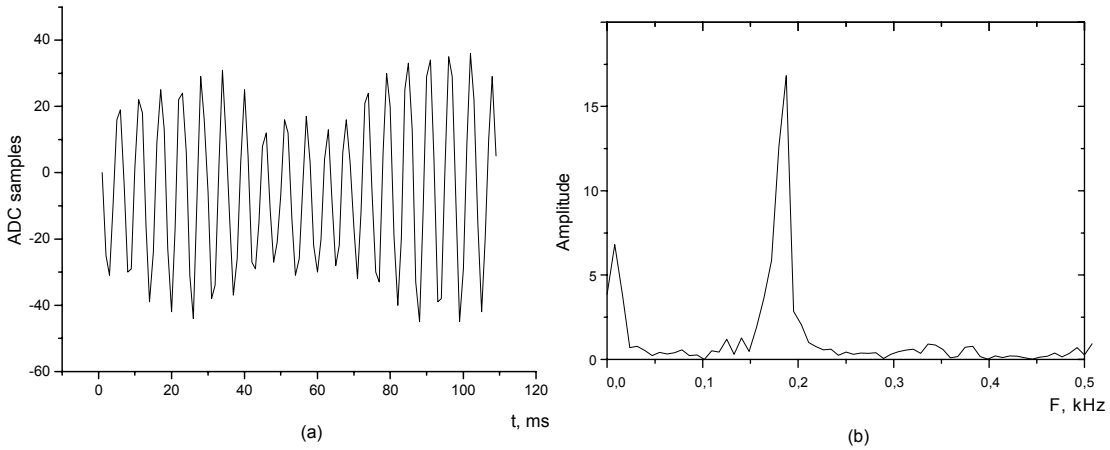

Figure 8: Doppler-Effect Signal Example Time Graph (a); its FFT (b)

Conclusion

The ultrasound motion detection sensor has been presented. The sensor can be used for building various intelligent devices, including home, office and car security systems, intellectual toys, and home appliances. The software sources, schematics, and board layout reference design simplify sensor adaptation for concrete application demands. The associated project includes full schematic and board layout files in Cadence Orcad 9.2. Note that the layout was performed for components on hand. Using smaller footprint components will allow user to build the sensor with noticeably smaller dimensions.

About the Author

Name:	Victor Kremin
Title:	Associate Professor
Background:	Victor earned radiophysics diploma in 1996 from Ivan Franko National Lviv University, PhD degree in Computer Aided Design systems in 2000 and is presently working as Associate Professor at National University "Lvivska Polytechnika" (Ukraine). His interests involve the full cycle of embedded systems design including various processors, operation systems and target applications. You may reach him at vkremin@polynet.lviv.ua
Contact:	Kerechenska str. 9-44, Lviv, 79035, Ukraine. vkremin@polynet.lviv.ua

Appendix

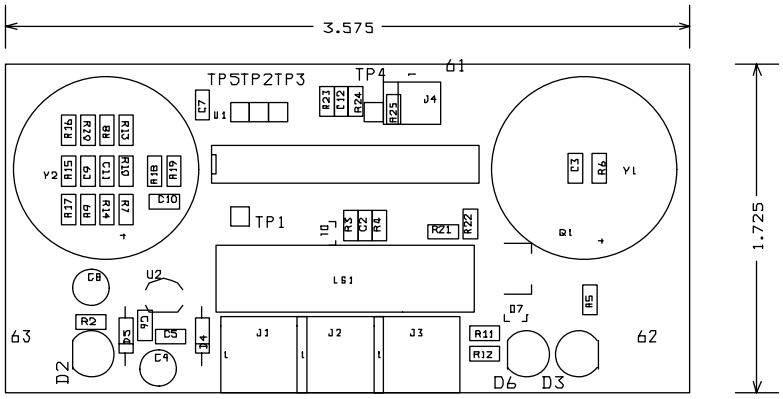

Component labels (dimensions are in inches)

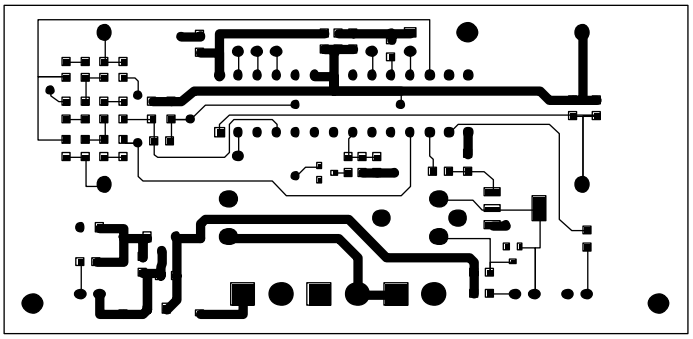

Top layout layer

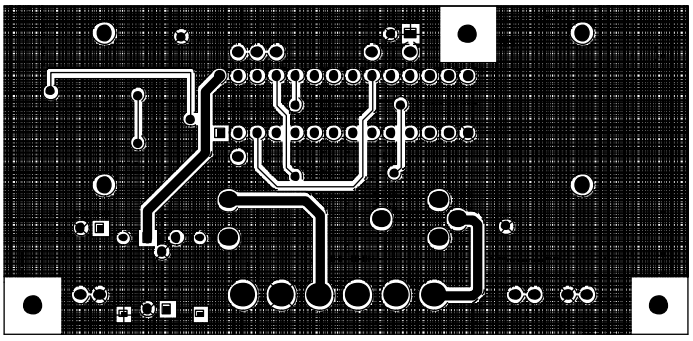

Bottom layout layer

Figure 9: Component Placement Layer and Board Layout Layers, Actual Size

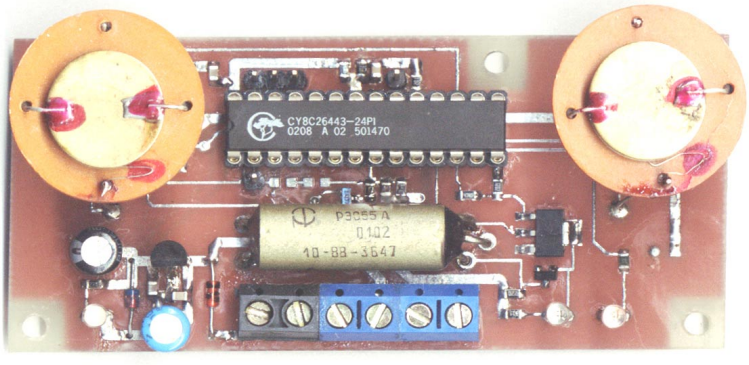

Figure 10: Sensor Photograph, Actual Size

Cypress MicroSystems, Inc.
22027 17th Avenue S.E. Suite 201
Bothell, WA 98021
Phone: 877.751.6100
Fax: 425.939.0999
http://www.cypressmicro.com/ / http://www.cypress.com/aboutus/sales_locations.cfm / support@cypressmicro.com